REPORT DOCUMENTATION PAGE

AFRL-SR-AR-TR-05-

0421

1. REPORT DATE (DD-MM-YYYY)	2. REPORT TYPE	3. DATES COVERED (From - To)
27-5-2005	FINAL	Sept. 2001-Feb.2005

4. TITLE AND SUBTITLE

Investigations of Optical Limiting Involving Light-Matter Interactions

5a. CONTRACT NUMBER

5b. GRANT NUMBER
AFOSR F49620-01-1-0553

5c. PROGRAM ELEMENT NUMBER

6. AUTHOR(S)

M. J. Potasek

5d. PROJECT NUMBER

5e. TASK NUMBER

5f. WORK UNIT NUMBER

7. PERFORMING ORGANIZATION NAME(S) AND ADDRESS(ES)

City College of the City University of New York
Dept of Physics
138th St and Convent Ave.
Rm 417
New York, NY 10031

8. PERFORMING ORGANIZATION REPORT NUMBER

9. SPONSORING / MONITORING AGENCY NAME(S) AND ADDRESS(ES)

Air Force Office Scientific Research/NM
875 N. Randolph
Ste. 325, RM 3112
Arlington, VA 22203

10. SPONSOR/MONITOR'S ACRONYM(S)

11. SPONSOR/MONITOR'S REPORT NUMBER(S)

12. DISTRIBUTION / AVAILABILITY STATEMENT

unlimited

Approved for public release, distribution unlimited

13. SUPPLEMENTARY NOTES

14. ABSTRACT

An optical limiter keeps the power, intensity, energy or energy density transmitted by an optical system below a predetermined maximum value that is independent of the size of the input pulse while maintaining a high transmittance at low input power. The many applications of the device include laser power regulation, laser mode-locking, optical pulse shaping, signal level processing, and sensor/detector protection. Important applications include protection of sensors, such as human eyes of pilots and photodetectors, from laser damage. In order to determine the parameters required for optimization of optical limiters, we are developing an extremely sophisticated numerical code. Additionally, new materials are needed with increased nonlinearity. Thus we also calculate the imaginary part of the third order optical non-linearity for an array of semiconductor quantum dots in an organic host and show that it leads to large two-photon absorption. The calculated two-photon absorption is greater than currently measured materials. The large non-linearity results from a hybrid exciton formed in the inorganic-organic medium. The band gap of the semiconductor dot determines the spectral region of the resonances that vary from the visible to the near, mid and far infrared regions. We show that relatively small changes in the ratio of the quantum dot size to the quantum dot-to-dot spacing result in significant changes in the non-linearity. We briefly describe applications in communications, optical filters, and bio photonics for thin films comprising these hybrid excitons

15. SUBJECT TERMS

lasers, hybrid excitons, quantum dots, nonlinear materials

16. SECURITY CLASSIFICATION OF:			17. LIMITATION OF ABSTRACT	18. NUMBER OF PAGES	19a. NAME OF RESPONSIBLE PERSON
a. REPORT	b. ABSTRACT	c. THIS PAGE			Dr. M. J. Potasek
U	U	U	none	26	19b. TELEPHONE NUMBER (include area code) 212-650-6823

May 27, 2005

FINAL REPORT

September 30, 2001-February 2005

Title: *Investigations of Optical Limiting Involving Light-Matter Interactions*

AFOSR grant: F49620-01-1-0553

Mary Potasek

Dept of Physics
City College of New York
New York, N. Y. 10031

Abstract

An optical limiter keeps the power, intensity, energy or energy density transmitted by an optical system below a predetermined maximum value that is independent of the size of the input pulse while maintaining a high transmittance at low input power. The many applications of the device include laser power regulation, laser mode-locking, optical pulse shaping, signal level processing, and sensor/detector protection. Important applications include protection of sensors, such as human eyes of pilots and photodetectors, from laser damage. In order to determine the parameters required for optimization of optical limiters, we are developing an extremely sophisticated numerical code.

Additionally, new materials are needed with increased nonlinearity. Thus we also calculate the imaginary part of the third order optical non-linearity for an array of semiconductor quantum dots in an organic host and show that it leads to large two-photon absorption. The calculated two-photon absorption is greater than currently measured materials. The large non-linearity results from a hybrid exciton formed in the inorganic-organic medium. The band gap of the semiconductor dot determines the spectral region of the resonances that vary from the visible to the near, mid and far infrared regions. We show that relatively small changes in the ratio of the quantum dot size to the quantum dot-to-dot spacing result in significant changes in the non-linearity. We briefly describe applications in communications, optical filters, and bio photonics for thin films comprising these hybrid excitons

Contents

1. Introduction

In general, an optical limiter keeps the power, intensity, energy or energy density transmitted by an optical system below a predetermined maximum value that is independent of the size of the input pulse while maintaining a high transmittance at low input power. The many applications of the device include laser power regulation, laser mode-locking, optical pulse shaping, signal level processing, and sensor/detector protection. Important applications to the Air Force include protection of sensors, such as human eyes of pilots and photodetectors, from laser damage. In order to determine the parameters required for optimization of optical limiters, we are developing an extremely sophisticated numerical code.

Because of its modularity and sophisticated algorithms this code has wide ranging future applications in medical optics, nanooptics, signal processing, multimedia, infomatics, medical imaging, laser damage, photonic crystals and industrial devices. Therefore it has potential uses in both the military and civilian domains. Additionally, the unique ways in which the code is modularized and the algorithms performed have important Intellectual Property consequences. We believe that the methods used here are unique. The potential applications of the numerical code could provide numerous new devices. This factor is significant for both the military and civilian domains.

Optical limiting now requires a vast set of properties including various nonlinear materials, different physical processes, various device designs including a number of lenses and other optical devices, optical pulse shaping, and the characteristics of the laser source including wavelength, pulse duration and pulse repetition rate. This range of materials, processes, and devices involve complex optical propagation requiring a large diversity of parameters that cannot be fully analyzed without the use of various numerical codes. Along with new materials and device structures, new numerical codes will be key elements in the development of optical limiters. Numerical investigation will be required to make additional advances by examining the various combinations of material, physical, and device parameters that would be too time consuming and/or costly to perform in the laboratory.

Therefore one of the key features to the successful design of future optical limiting systems will be sophisticated numerical codes. As stated previously, the increasing complexity of the materials, device geometry, and optical beam shaping and signal processing necessitates the use of numerical simulation for system optimization. The number of variable parameters that will have to be optimized can approach fifty (50) different variables. Clearly it is not time nor cost efficient to perform all of these variations experimentally. The numerical codes will also further guide quantum mechanical calculations and molecular engineering in order to optimize the possible molecular structure of the nonlinear material. This code is modular so that the functions can be reused or eliminated as desired. This can be a significant feature in such a highly complex code. Furthermore it should be possible to use additional visualization tools such as animation that could enhance the understanding of the optical limiting process and enable novel advances in the science and technology.

A second area of investigation involves new materials. Accelerated growth in nanotechnology has led to materials with unique physical and optical properties that have never been observed before. These developments have given rise to potential applications and devices with physical properties that can far exceed those of traditional

materials/systems. Advances in colloidal chemistry have enabled a technology to create large numbers of semiconductor quantum dots. The semiconductor dots can be deposited in close-packed films using organometallic synthesis. Recently, large-scale three-dimensional arrays of semiconductor dots in an organic medium have been synthesized and used in electron transport studies of films. These advancements in synthesis techniques hold promise for creating other classes of devices with different electrical and nonlinear optical properties.

2. Description of the Methodology

Because of the complexity of the beam propagation in optical limiting systems numerical methods must be used. The numerical methods for solving the optical propagation along the path from the incident beam to the detector can be divided into the parts shown in Fig. 1.

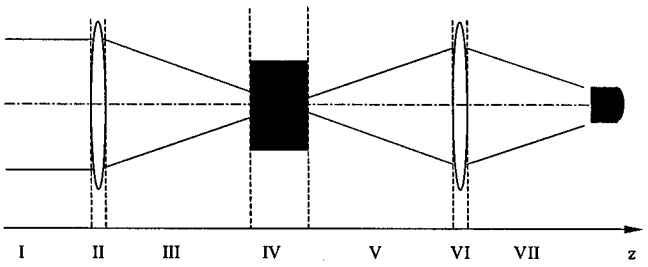

Figure 1. Schematic diagram of the system.

This figure demonstrates the simplest optical limiting device that uses a single nonlinear element; however, in many real situations additional lenses, limiting materials, and apertures (not include in this figure) could be included. Region I shows the incident beam. Regions II and VI are thin lenses where the field propagation can be calculated using a simple phase shift. After propagating through the first lens, the beam is still Gaussian shaped. Therefore in Region III the only difference in the field is the beam waist. Region IV contains the nonlinear material through which the propagation of the field may include nonlinear absorption, nonlinear refraction, and dispersion. However, after propagation through the nonlinear medium the emerging beam is usually no longer Gaussian shaped and the Huygen-Fresnel propagation formalism is required for beam propagation in regions V and VII.

2.1. Regions I-III

The paraxial wave equation of Gaussian beam can be written as

$$A(r,\tau,z') = \frac{A_0 e^{-i\phi(z')}}{\sqrt{1+z'^2/z_0^2}} e^{ikr^2/2R(z')} e^{-r^2/w^2(z')} e^{-\tau^2/\tau_0^2}$$

$$\phi(z') = \tan^{-1}(z'/z_0)$$

$$R(z') = z' + \frac{z_0^2}{z'} \qquad (1)$$

$$w(z') = w_0\sqrt{1+z'^2/z_0^2}$$

where $z_0 = \frac{\pi w_0^2}{\lambda}$ is Rayleigh range, also known as confocal parameter, z' is defined as the distance to the Gaussian beam waist in the beam propagation direction, w_0 is the radial beam waist , r is the transverse coordinate.

A Gaussian beam passing through a lens maintains its Gaussian shape because the intensity distribution is unchanged by a thin lens. By considering the incident Gaussian beam as a spherical wave, the output can be obtained by solving the ray matrix using the ABCD law. After the lens, the emergent Gaussian beam will have a new radial beam waist and location given by

$$d = \frac{f}{1+f^2/z_0^2}$$

$$w_0' = \frac{\lambda f}{\pi w_0}\frac{1}{\sqrt{1+f^2/z_0^2}}, \qquad (2)$$

where d is the distance to the beam waist after the lens. This equation describes focusing a collimated beam. Written in terms of the $f^{\#}$ ($f^{\#} = f/2w_0$), Eq (2) becomes

$$d = \frac{2w_0 f^{\#}}{1+(2w_0 f^{\#})^2/z_0^2}$$

$$w_0' = \frac{2\lambda f^{\#}}{\pi}\frac{1}{\sqrt{1+(2w_0 f^{\#})^2/z_0^2}} \qquad (3)$$

The f-number is often f/5-f/10. In Fig. 1, d is the distance from the first lens to the focal plane in the medium. Therefore the focal plane can be adjusted from the incident plane to the exit plane in order to best utilize the nonlinear material. The beam waist w_0' is assumed to be a collimated beam that could be incident from far away. The choice of the placement of the focal plane could also be significant in multiple nonlinear element

designs. In some cases, it may be beneficial to have multiple elements to provide optical limiting for multiple wavelengths and/or multiple pulses.

2.2 Region IV

This is a single or multiple element nonlinear material that performs the functions of beam shaping and nonlinear absorption. In the nonlinear material, the propagation operator along the z-axis is written as

$$A(r,\tau,z+\Delta z)=\exp\left[-i\Delta z\hat{Z}(r,\tau,z)\right]A(r,\tau,z)$$

$$\hat{Z}(r,\tau,z)=\frac{1}{2k}\left[\frac{\partial^2}{\partial r^2}+\frac{1}{r}\frac{\partial}{\partial r}-ik\alpha_L+k_0^2\chi_{NL}(r,\tau,z)+k\,k_2\frac{\partial^2}{\partial\tau^2}\right] \tag{4}$$

A unique feature of our code is that it discretizes the propagation in both the temporal and spatial domains so that all temporal and spatial effects can be observed. In this respect it is the most detailed code to date. Additionally, the RSA material was treated as a five-level model, instead of the three-level model approximation used in previous calculations. The linear operator is given by

$$\hat{Z}_L=\frac{i}{2k}\left(\frac{\partial^2}{\partial r^2}+\frac{1}{r}\frac{\partial}{\partial r}\right)-\frac{ik_2}{2}\frac{\partial^2}{\partial^2\tau}\,. \tag{5}$$

The nonlinear operator is given by

$$\hat{Z}_{NL}(r,\tau,z)=-\frac{\alpha_L}{2}-i\frac{k_0}{2n_0}\chi_{NL}\,. \tag{6}$$

The propagation equations are discretized in radial, temporal and propagation directions. This method enables determination of all spatial and temporal features of the beam propagation through the entire optical system. Thus additional features may be observed with this code that are not possible with other codes.

2.3. Regions V and VII

According to the Huygens-Frensel Principle (HF), every point of the wavefront can be considered a new wave source that mutually interferes with one another. Using the paraxial approximation and the HF, the field can be expressed as a plane wave given by

$$A(z+\Delta z,r,\tau)=\frac{k}{i\Delta z}\exp\left(\frac{ikr^2}{2\Delta z}\right)\int_0^\infty r'dr'A(z,r',\tau)\exp\left(\frac{ikr'^2}{2\Delta z}\right)J_0\left(\frac{krr'}{\Delta z}\right) \tag{7}$$

where J_0 is zero order Bessel function and Δz does not need to be small.

2.4 Region VI

For the thin lens, in the paraxial approximation the only change to the field is the phase. The field after the lens is simply expressed as

$$A'(z,r,\tau) = A(z,r,\tau)\exp\left(-\frac{ikr^2}{2f}\right) \tag{8}$$

where f is the focal length.

3. Effects of Optical Pulse Trains

To date numerical codes consider only a single incident pulse. Yet most lasers emit trains of pulses and cw lasers can be externally modulated to create optical pulse trains. Therefore it is of interest to consider the effect of pulse trains on optical limiters. A schematic diagram of a train of pulses incident to an optical limiter is shown in Fig. 2.

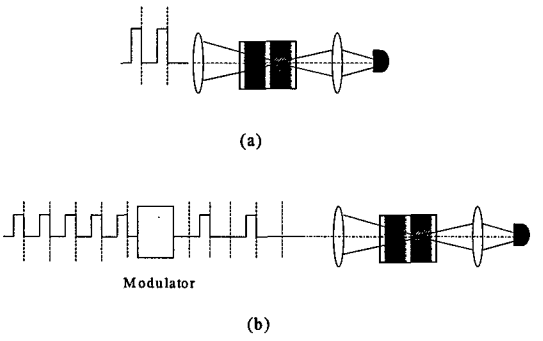

Figure 2. Schematic diagram of pulse trains incident on an optical limiter. (a) regularly modulated pulse train, (b) randomly modulated pulse train.

The equation for the incident pulse train is given by

$$A(0,\tau) = \sum_{k=1}^{N} A_0 \exp\left[\frac{-(\tau - k\tau_R)^2}{\tau_0^2}\right] \tag{9}$$

where τ_R is the repetition rate. If an external modulator is used, then the pulse train can be randomly modulated as shown in Fig. 22 (b). The equation for this case is given by

$$A(0,\tau) = \sum_{k=1}^{N} A_0 b_k \exp\left[\frac{-(\tau - k\tau_R)^2}{\tau_0^2}\right] \tag{10}$$

where b_k =0 or 1 depending on whether the kth pulse slot contains a pulse or not.

3.1 Investigation of Multiple Pulses

The use and significance of multiple pulses is increasing in many situations. In addition to traditional methods such as mode-locking or Q-switching, other techniques are possible for creating pulse trains with a wide range of repetition rates and pulse widths using optical modulators, beam splitters, optical delay lines and booster amplifiers. Our model and numerical method is applicable to a wide range of excitation conditions however, here we have investigated pulse trains from 5 to 20 pulses at two different pulse widths; namely, 40 ps and 1 ns (1/e half width). The two different pulse widths were selected in order to demonstrate and validate the pulse width dependence on the intersystem crossing rate of the molecular system. Since we found that there was little difference in the general physical results when we varied the number of pulses, we present results for five pulses as examples.

The physical values used for our calculations are taken from the literature for the class of phthalocyanine molecules considered: $\sigma_{01}=2.4\text{x}10^{-18}$ cm^2, $\sigma_{12}=3.0\text{x}10^{-17}$ cm^2, $\sigma_{34}=4.8\text{x}10^{-17}$ cm^2, $k_{10}=0.144$ ns^{-1}, $k_{21}=1.0$ ps^{-1}, $k_{13}=77.8$ μs^{-1}, $k_{30}=50.0$ ms^{-1}, $k_{43}=1.0$ ps^{-1}. The other parameters used in our calculation are N_T (0.0048 nm^{-3}), beam waist (40 μm), wavelength (532 nm) and material thickness (0.6 mm).

The damage threshold for various photo detectors, including the cornea, can exhibit repetition rate dependence. To protect such detectors, optical limiters will need to be developed that are operable at high repetition rates or when subjected to complex excitations. Recent Z-scan experimental investigations have shown that multiple pulse excitation of some of the materials being investigated for optical limiters display dramatically different behavior than single pulse excitation. As lasers become more intense and exhibit increased repetition rates, a detailed quantitative description is required to describe the transient response of the material. Fig. 3 shows the input intensity normalized to I_o as a function of time normalized to t_o.

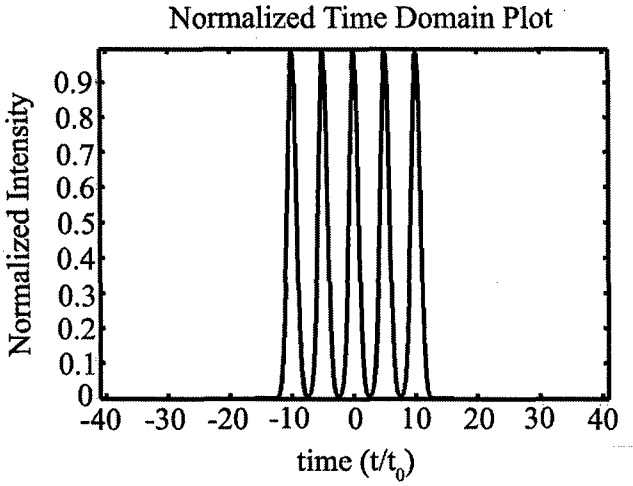

Fig. 3. Normalized pulse intensity as a function of time at the input to the material.

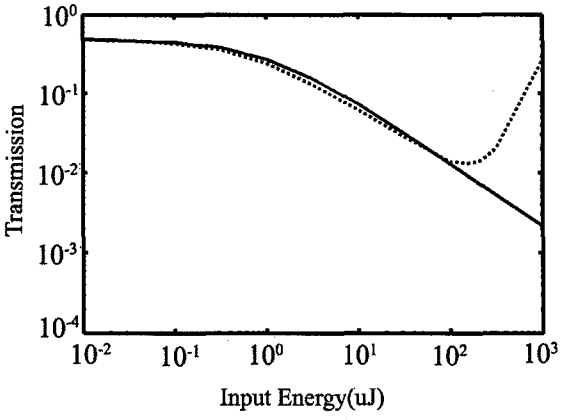

Fig. 4. Transmission curve as a function of input energy into the phthalocyanine chromophore for five pulses with pulse half-widths of 1 ns (solid line) and 40 ps (dashed line), pulse separation, t_r =5 and L=0.6 mm.

Fig 4 shows the transmission curve vs. input energy for both the 1 nsec pulse sequence and the 40 psec pulse sequence. Transmission is defined as the output intensity integrated over r and t divided by the input intensity integrated over r and t. The transmission decreases with increasing energy for both pulse width sequences within the range of 0.01 μJ to 100 μJ due to excited state absorption (reverse saturable absorption - RSA). Beyond 100 μJ, the 40 psec pulse sequence experiences saturation whereas the nsec pulse sequence does not. The onset of saturation around 100 μJ for the psec case is due to the depletion of ground state population, which reduces the excited state absorption. Intersystem crossing experienced by the nanosecond pulses enables the continued RSA. Since the relaxation time from level (3) to level (1) is about 0.02 ms, the successive transfer of population from level (3) to level (4) is possible with the optical pumping for the nanosecond pulses. Since the excited state absorption cross-section σ_{34} is larger than that of the ground state absorption cross-section σ_{01}, more light is absorbed if the population has accumulated at level (3). These effects contribute to the nonlinear absorption up to 1mJ for the nanosecond pulses.

3.2 Investigation of temporal and radial domains

Next we investigate the temporal pulse shapes. Fig. 5 (a) shows the output pulse intensities for 40 ps and 1 ns pulse sequences as a function of time and radius for various input energies. The first energy shown is 0.01 μJ, which we can see from Fig. 4 corresponds to the linear absorption region. In this case the normalized peak intensity for each of the pulses is 0.45 in agreement with Fig. 4. The next input energy is 3.16 μJ and

both the 40 ps and the 1 ns pulse sequences show similar behavior, which is the onset of RSA. At this onset of RSA, it is interesting to note that the trailing pulses are more absorbed than the leading pulses because of the accumulation of population in state 1 due to the leading pulses. This cumulative effect results from the long decay rate of level 1. Since the excited state absorption cross section is larger than that of the ground state, there is more than enough population in the excited state to allow the trailing pulses to be excited to the next level, which causes more and more absorption of energy from the trailing pulses. At an input energy of 100 μ J we see the onset of saturation for the 40 ps pulse sequence and at 1000 μ J the transmission returns to the linear absorption, which is in agreement with Fig. 4. However, the behavior of the 1 ns pulse sequence is different. It does not saturate and we continue to see the decay of the trailing pulses even at 1000 μ J input.

We now examine the behavior of the intensity as a function of radius for the same input energies as above. This is shown in Fig. 5 (b) where we plot the intensity of the central pulse after it exits the material as a function radius for various input energies. At an input energy of 0.01 μ J the transmission value is 0.45 in agreement with Fig. 4. As the input energy increases (e.g. 32 μ J) the intensity decreases and the pulse profile begins to flatten in the radial domain. However at 100 μ J, the 40 ps pulse shows a small increase at its center. This energy value corresponds to the minimum transmission value for the 40 ps curve in Fig. 4. Comparison of the corresponding curve for the 1 ns shows that the intensity does not exhibit this increase in the center of the pulse. Then at 1000 μ J we see that the 40 ps pulse transmission corresponds to the linear absorption value; while the 1 ns pulse remains low. The radial domain plots clearly demonstrate the effects of saturation shown in Fig.4. Therefore both the temporal and spatial domains contain significant information about the laser-matter interaction.

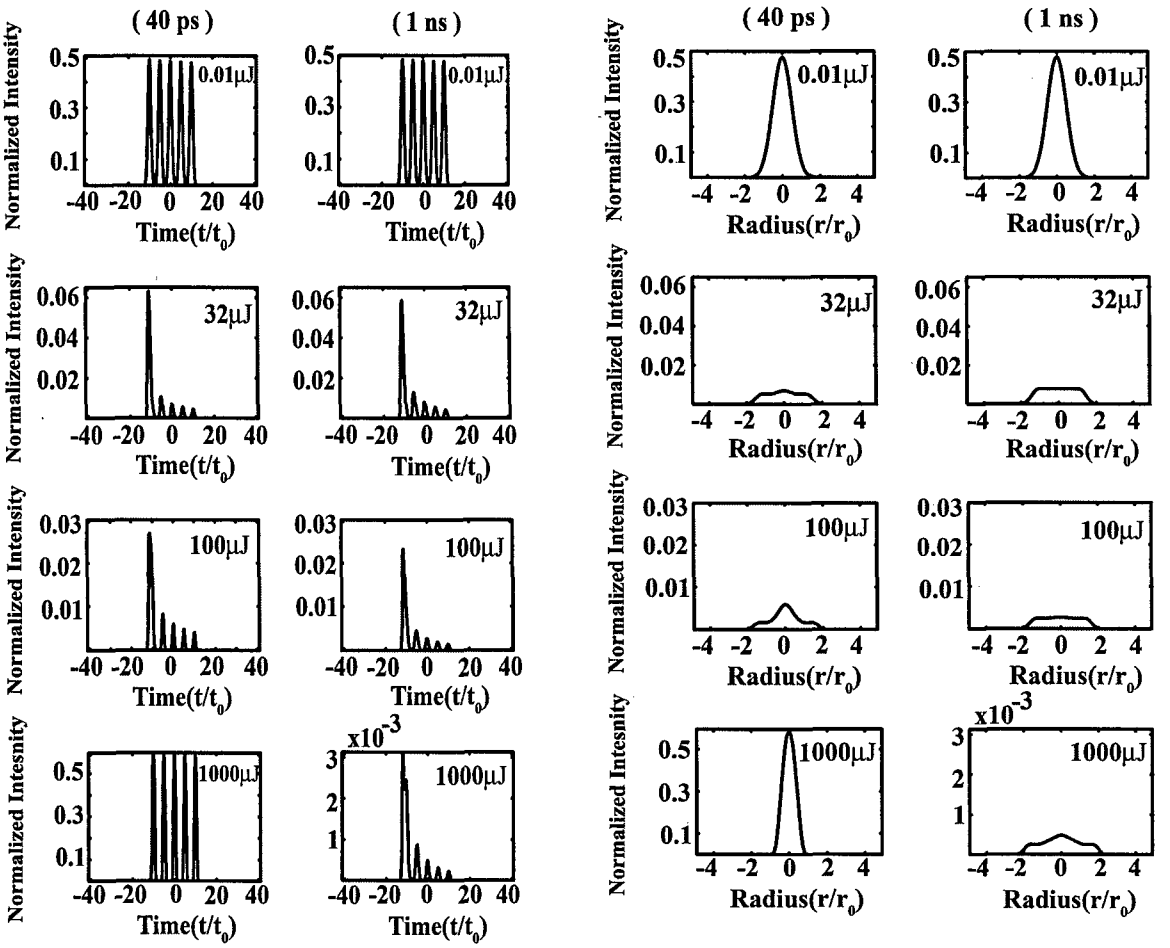

Fig. 5 (a) Normalized pulse intensity as a function of time at the output of the material for five pulses with pulse half-widths of 1 ns and pulse separation, t_r =5 and r=0. (b). Normalized pulse intensity as a function of radius at the output of the material for five pulses with pulse half-widths of 40 ps and 1 ns and pulse separation, t_r =5 and t=0.

The population densities vs. time and radius are shown in Fig. 6 and Fig. 7 for the 40 psec excitation sequence. The populations of levels 3 and 4 remain negligible and are not shown. The input energy corresponds to the onset of saturation, 100 μJ. Fig. 5 shows that the population density of state 1 accumulates with successive pulses. The shape of the population density vs. radius for state 2 becomes distorted with successive pulses and this is shown in Fig. 7 (a). Fig. 7 (b) shows a detail of the radial distortion for the center pulse in the sequence.

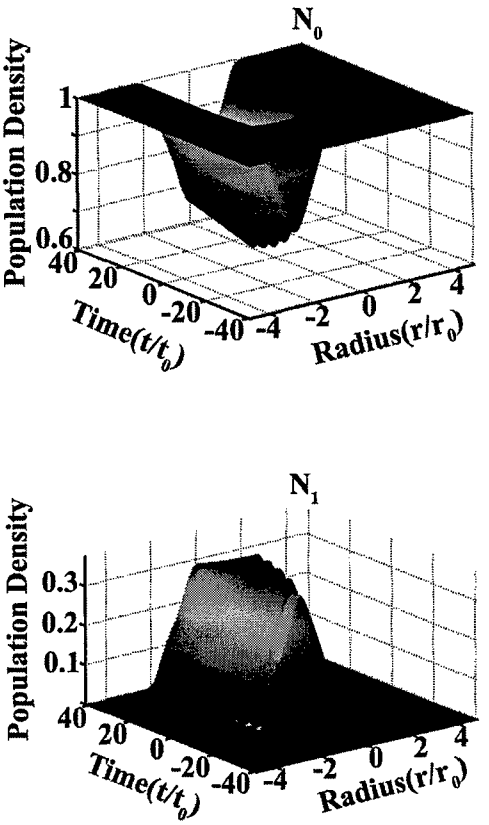

Fig. 6 Population densities for levels N_0 and N_1 as functions of time and radius.

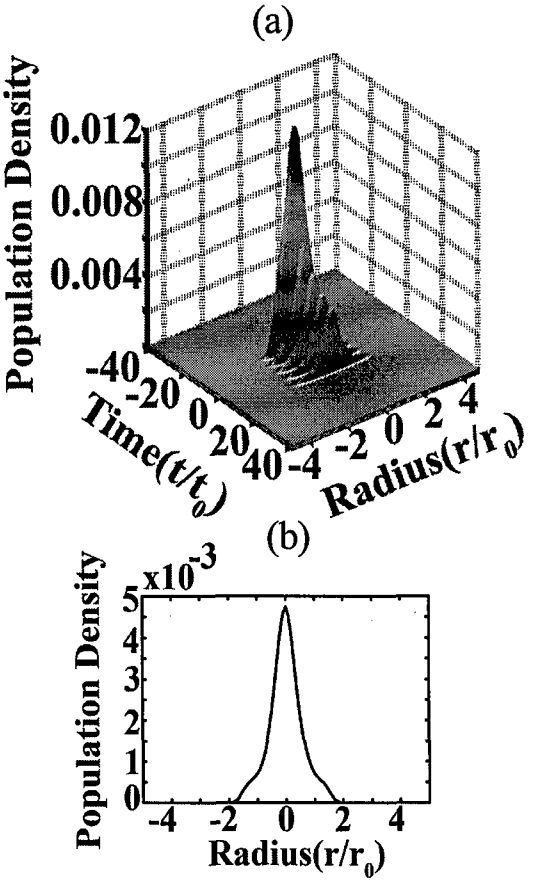

Fig. 7. Population densities for N_2. (a) three dimensional plot of intensity as function of radius and time. (b) plot of intensity as function of radius for the center pulse in the pulse sequence.

Our analysis demonstrates that changes in the radial domain need to be considered in order to understand and characterize the laser matter interaction. This particular aspect of the analysis is traditionally omitted from other numerical procedures yet; we show that the radial changes can be significant.

4. Semiconductor quantum dot lattices

4.1 Description

Recent results show that semiconductor dot three-dimensional arrays in organic media lead to enhance nonlinear third order optical susceptibilities. When semiconductor quantum dots are placed in a three-dimensional lattice, the excitons in nearest-neighbor quantum dots interact with each other due to multipole interaction. This interaction allows the presence of a "transfer Wannier-Mott exciton " propagating through the lattice. The presence of this transfer exciton helps to increase the optical nonlinearity of the single quantum dots to overcome the limitation of the single dot size effect. When such a lattice is put in an organic host, this transfer Wannier exciton is coupled with the Frenkel exciton of the organic medium and at resonance of the two excitons, a hybrid exciton appears in the system. The mixed state has a large exciton radius, large oscillator strength and very large optical nonlinearity. The lattice configuration allows tuning the optical properties and resonance regions as well as the value of the nonlinearity by controlling the dot radius, the spacing between the dots, and the material, especially the semiconductor dot band gap, used for the hybrid arrays.

The role of systems with large optical nonlinearity is growing in importance. Important recent developments in technology have created faster and more intense lasers, from the visible to the far infrared thus enabling multiphoton processes across a broad range of wavelengths from the visible (~0.4-0.6 μm) to the short (0.8-2 μm), mid (3-8 μm) and far (>12 μm) infrared spectral regions. Two photon processes are particularly useful in many applications including fluorescence imaging, optical data storage, micro fabrication, photoconductors and photovoltaics, markers for genomes and proteins, biological and medical detectors, optical limiters, biomimetric electromagnetic devices and nanopatterning of inorganic/organic materials. Consequently, we investigated the two-photon absorption properties of this array of semiconductor dots in organic materials with its hybrid exciton.

4.2 Hybrid-Exciton

The property of this hybrid exciton formed by combining the "localized" Frenkel exciton with a "delocalized" Wannier-Mott exciton has been of considerable recent interest. The Frenkel exciton is the excited electronic state with the electron and the hole situated in the same molecule or atom. The Frenkel excitons have small radii and very large oscillator strength. In constrast, being a pair of electron and hole in the semiconductors, the large-radius Wannier-Mott exciton in semiconductors is relatively weakly bound due to typically large electron-hole distance. The interaction between Wannier-Mott excitons is very important while their oscillator strength is rather weak. The Wannier-Mott exciton wavefunctions overlap each other to get the exciton resonance, so the optical nonlinearity of Wannier-Mott exciton can be large at rather low

density. These differences between the Frenkel excitons in organic materials and the Wannier excitons in semiconductors suggest forming systems, which have a hybridization of both the excitons. By combining an organic material and a semiconductor in one heterostructure system, an excitation state is expected to have major properties of both kind of excitons and can overcome the limitation of each kind of excitons. Quantum dots have attracted a lot of attention because of their three-dimensional confinement. The electronic structure and optical properties of quantum dots depend sensitively on the size of these zero-dimensional nanocrystals. As a result of the confinement effect on the exciton energy levels, the oscillator strength of optical transitions in quantum dots increases with the size of crystallites and is very large in comparison with the bulk, leading to an increase of the optical nonlinearity.

For an ideal lattice of same-sized quantum dots placed in an organic medium, the total Hamiltonian is given by:

$$H = \sum_{nl} E_{nl}^{W}(k) a_{nl}^{+} a_{nl} + \sum_{km} E_{m}^{F}(k) b_{km}^{+} b_{km} + \sum_{nlmk} g_{nlm}(k)(a_{nl}^{+} b_{km} + a_{nl} b_{km}^{+}) + \sum_{nn'll'} t_{nn'll'}(k)(a_{nl}^{+} a_{n'l'} + h.c.) \quad (11)$$

where $g_{nlm}(k)$ is the coupling constant of Wannier exciton and Frenkel excitons, and $t_{nn'll'}(k)$ is the hopping constant between excitons in nearest dots, a_{nl}^{+}, a_{nl} (b_{km}^{+}, b_{km}) are creation and annihilation of Wannier (Frenkel) excitons, respectively, l labels the exciton states and $n = \{i, j, h\}$ label the sites in the quantum dot lattice, E_{nl}^{W} and E_{m}^{F} are the energies of the Wannier excitons in the dots and the Frenkel exciton in the medium, respectively.

The Hamiltonian (Eq. (1)) consists of the free Wannier and Frenkel exciton term, the Wannier-Frenkel exciton coupling term and hopping term between the Wannier excitons in nearest dots. Due to confinement, the Wannier exciton energy in the dot has discrete value according to the zeros of the Bessel functions.

The hybrid exciton has the energy:

$$E(k) = \tfrac{1}{2}\{E^{F}(k) + E_{tr}^{W}(k)\} \pm \tfrac{1}{2}\{[E^{F}(k) - E_{tr}^{W}(k)]^{2} + 4G^{2}(k)\}^{1/2} \quad (12)$$

and the wavefunction:

$$\Psi(k) = u_{l}(k) f^{F}(0) \Psi_{l}^{W}(k) + v_{l'}(k) f^{W}(0) \Psi_{l'}^{F}(k) \quad (13)$$

where $\Psi_{l}^{W}(k), \Psi_{l}^{F}(k)$ are excited states, $f^{W}(0), f^{F}(0)$ are ground states of the Wannier and Frenkel excitons and $u_{l}(k)$ and $v_{l'}(k)$ are Bogoliubov transformation coefficients. The Wannier-Frenkel exciton coupling constant $G(k) = < F(k) | H_{\text{int}} | W(k) >$, where H_{int} is the coupling of the field created in the organic medium by the exciton in the quantum dot with the transition polarization operator of the organic medium, and the hopping constant $t(k) = < W_{i}(k) | H_{d-d} | W_{j}(k) >$ where H_{d-d} is the dipole-dipole interaction between two dipole moments in the two

nearest dots and $W_i(k)$ is the wavefunction of the exciton in the dot have been calculated in detail. The energy and the optical properties of the hybrid exciton depend strongly on the values of $G(k)$ and t(k).

In the region of mixing, both the Wannier and Frenkel excitons contribute to the oscillator strength of the hybrid exciton. And one of the strong points of this model is its ablity to tune the resonance by changing the materials and the parameters of the system to obtain the desired resonance region value and non-linearity values. For example, by choosing a semiconductor with a band gap in the region of 2.5 eV, large optical third order non-linearities can be obtained at wavelengths in the visible and near IR spectral region where many lasers exist, such as the Nd:YAG laser (1064 nm) which can be frequency doubled (520 nm) and tripled (355nm). In these spectral regions, there are many applications for materials with large optical non-linearities, such as optical communications (e.g. optical switches) and laser hardening (e.g. optical filters and optical limiters). Both the real and imaginary parts of the non-linearity are potentially of interest. The real part gives rise to self-focusing or self-defocusing depending on the sign of the non-linearity; while, the imaginary part gives rise to two-photon absorption. Figs. 8 and 9 show schematic diagrams of thin film structures of inorganic-organic materials. Fig. 8 shows one type of semiconductor in an organic medium and Fig. 9shows a multi-layered structure in which different semiconductors are used. For example, one layer may be a self-focusing layer and the other layer may be a two-photon absorbing layer. Various materials and structures may be used for different applications.

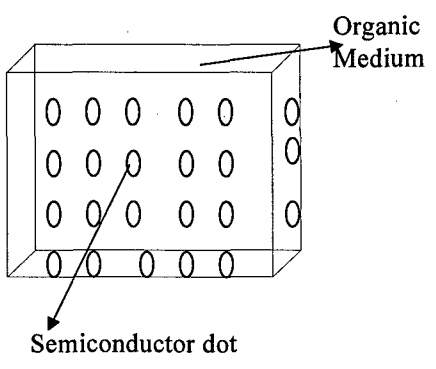

Fig. 8. Schematic diagram of a thin film organic-inorganic structure.

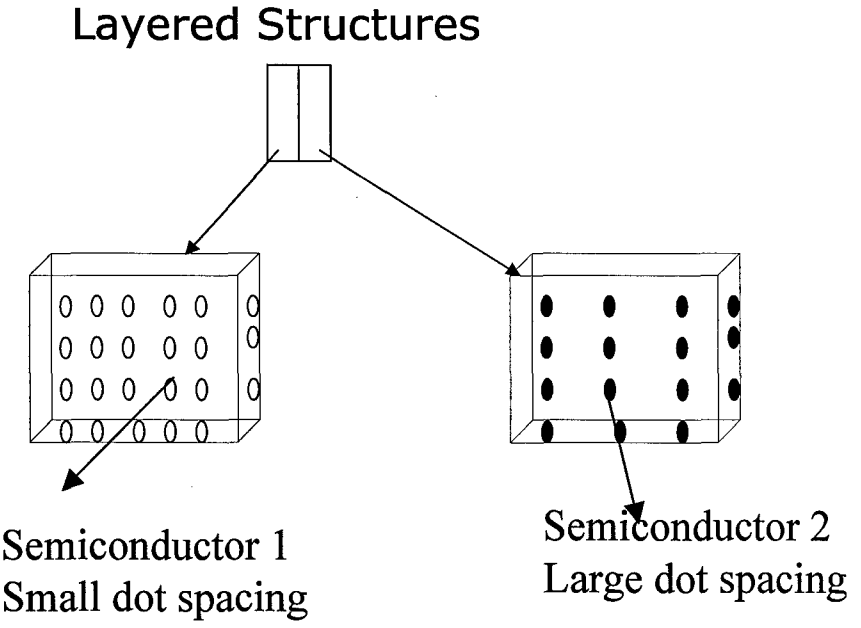

Fig. 9. Schematic diagram of a multi-layered thin film structure with different types of semiconductors and different dot spacing in each layer.

Due to the confinement effect of the exciton as well as the transfer exciton coupling between dots in the array, the Wannier transfer exciton may achieve the

oscillator strength comparable to that of Frenkel exciton, and so the hybrid exciton has very large oscillator strength. In the presence of an optical field, the third order susceptibility has been calculated using the standard perturbation theory. The increase of the oscillator strength as well as the increase of coherence length leads to a large figure merit of the hybrid exciton and the large nonlinearity. The imaginary part of the third order nonlinearity is given by

$$\mathrm{Im}\,\chi^{(3)} = \frac{\mu_F^4}{\varepsilon_0}\left(\frac{2\sqrt{2}}{\pi^2}\right)^4\left(\frac{V_m}{V_c}\right)^2 \ell_c^3\left(\frac{R}{d}\right)^6\left(\frac{1}{\pi a^3}\right)^2$$

$$\times\frac{(\omega-\varpi)^2(\gamma_\square-2\gamma_\perp)-\gamma_\perp^2\gamma_\square}{\hbar^3\left[(\omega-\varpi)^6+(\omega-\varpi)^4(\gamma_\square^2+2\gamma_\perp^2)+(\omega-\varpi)^2\gamma_\perp^3(2\gamma_\square-\gamma_\perp)+\gamma_\square^2\gamma_\perp^4\right]} \qquad (14)$$

where ℓ_c is the coherence length, $\gamma_\perp$ and $\gamma_\square$ are the transverse and longitudinal relaxation constants of the excitonic transition, respectively, R is the dot radius, d is the dot to dot separation, V_m is the volume of the organic host, V_c is the volume of one cell in the organic lattice, μ_F is the optical transition dipole moment of the organic molecule, a is the Bohr radius, and $\hbar\varpi$ is the lowest excitation energy of the hybrid exciton. The parameters used for the calculation are $\hbar\varpi$ = 25 meV (i.e. CdS), a = 30 Å, $V_C = (5\ \text{Å})^3$, $V_m = (5000\ \text{Å})^3$, μ_F = 5 D (1D=3.335x10^{-30} Coulomb.meter), $\gamma_\perp$=5.0x10^{12} s^{-1} and $\gamma_\square$=2.27x10^9 s^{-1}. Our calculations assumed CdS quantum dots with a dot size of about 30-100 Å and a dot-to-dot spacing ranging from 2 to 5 times the dot size.

5. Application of Hybrid Material

As one example of an application of these hybrid structures, we investigate their potential for optical power limiting or optical filtering. Figure 10 shows plots of the imaginary part of the third order nonlinear susceptibility as a function of wavelength. The resonances occur near 500 nm and the non-linearity is large even at off-resonance wavelengths including the near IR region. Future studies will investigate the real part of the non-linearity that gives rise to the nonlinear index of refraction coefficient. As stated previously self-focusing or self-defocusing results from the real part of the non-linearity. For example, very strong self-focusing may enable smaller spot size for laser induced micro fabrication. This may lead to improved methods for making nanostructures such as photonic crystals.

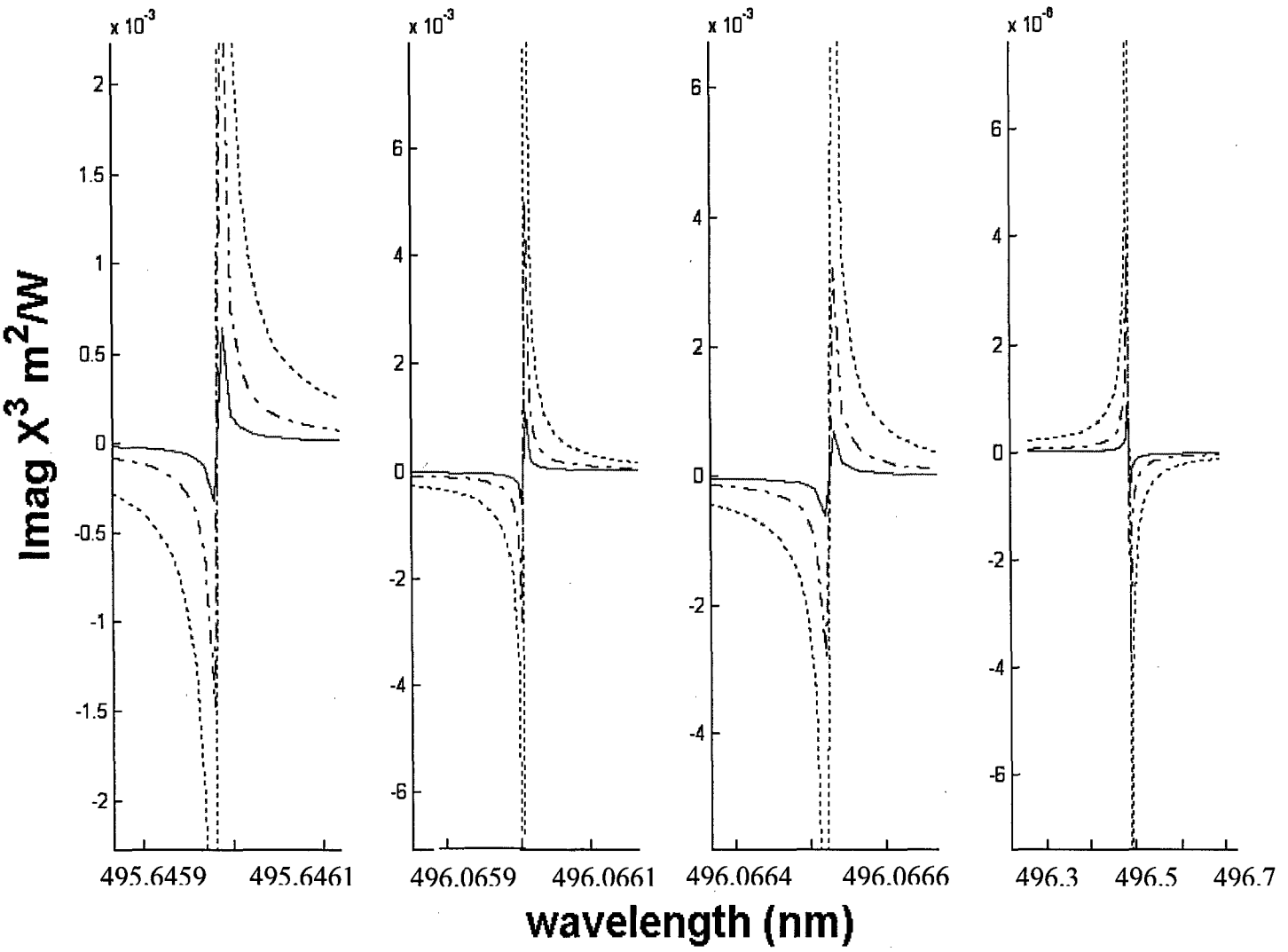

Fig. 10. Plots of Imaginary part of the third order nonlinear susceptibility as a function of wavelength. The dotted curves correspond to R= 50 A and d=100A, the dash dot curves correspond to R=50 A and d=150 A, and the solid curves correspond to R=40 A and d=160 A.

There are four resonances that occur in the visible spectral region. Fig. 10 shows the imaginary part of the third order susceptibility as a function of wavelength for three ratios of d/R; namely, d/R =2, 3, 4. Since quantum confinement restricts the size of the dot to ~3-10 nm, values between 4 nm and 5 nm were selected as initial examples. The curves show that as the ratio d/R increases the non-linearity decreases. At off-resonance wavelengths, our calculations show that about an order of magnitude (i.e. ~ factor of 10) increase in the non-linearity is possible when the d/R ratio is reduced by only a factor of 2 (e.g. from 4 to 2). Thus a significant change in the non-linearity can be achieved by relatively small changes in this ratio. These results indicate the ability to significantly tune the non-linearity by changing the d/R ratio. Further studies are required to examine the effects of various semiconductors and additional changes in the dot size and dot-to-dot distance.

Devices containing optical limiting materials are often used for laser protection in the visible and infrared spectral regions for optical (human eyes) and optoelectronic detectors. Many different types of materials have been investigated for optical limiters such as organics, fullerenes and semiconductors. With the recent advancements in laser technology, additional materials are required for optical limiters. Typical optical limiters in the visible and near infrared regions reduce the transmission of the incident laser beam by about an order of magnitude. Yet, for many applications, it is advantageous to have a single element that can reduce the transmitted energy by several orders of magnitude (~1000). An important physical mechanism used for optical limiting is two-photon absorption. The imaginary part of the susceptibility gives rise to the coefficient for two-photon absorption (a_2) and is given by

$$a_2 = \frac{3\omega_0}{4n_0 c}\,\mathrm{Im}\left(\chi^{(3)}\right) \tag{15}$$

At this time, our calculation of the two-photon absorption (a_2) coefficient, for the inorganic-organic material described in this paper, shows that it significantly exceeds (by two to five orders of magnitude) that of other traditional materials in the visible/near infrared spectral regions. Future work will investigate other materials for comparison.
For example, we obtain values of a_2 ~1.2 x10^{-9} m/W **{I}** for CdS quantum dots (R~100 Å, d~200 Å) in an organic medium at a wavelength of 800 nm. This value exceeds a_2 for other materials in the visible and near infrared spectral regions. For example, a_2 ~10^{-14} m/W **{II}** (532nm) for 2,2'-(9,9-dihexyl) bifluorene, a_2~6x10^{-11} m/W **{III}** (800nm) for green fluorescence protein, and a_2~10^{-11}m/W **{IV}** (1060nm) for trans-4-[p-(N-ethyl-N-hydroxethylamino)styrl]-N-methypyridinium tetraphenylborate.

Table I. Values of the two-photon absorption coefficient as a function of wavelength

Material	a_2 (m/W)	Wavelength (nm)
{I}	1.2×10^{-9}	800
{II}	1×10^{-14}	532
{III}	6×10^{-11}	800
{IV}	1×10^{-11}	1060

We calculated the transmission through a hybrid semiconductor dot-organic thin film using the two-photon absorption parameters obtained from Eq. (15). Potasek et. al. have developed theoretical models and numerical codes for laser pulse propagation in nonlinear absorbers. Using numerical simulation we calculated the transmission of a Gaussian laser beam through a hybrid 3D semiconductor array-organic film with a thickness of about 500 μm at an incident wavelength of 800 nm. The figure shows more than three orders of magnitude (>1000) reduction in transmission. This reduction is greater than that obtained using traditional materials.

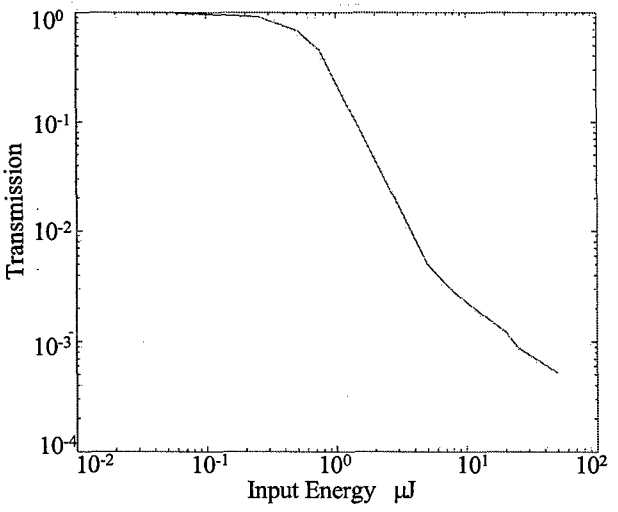

Fig.11 Transmission as function of input energy

6. Conclusions

Considerable new efforts were added to the investigation of nonlinear absorbers that are critical to laser protection. New advances in femtosecond lasers with short duration optical pulses and fast repetition rates increase the possibility of laser damage in this new regime. Our numerical effort has expanded into these new areas.

Additionally we show that an array of semiconductor quantum dots in an organic host leads to large two-photon absorption. The optical nonlinearity depends on the semiconductor, the dot size and the dot-to-dot spacing. Using numerical simulations, we demonstrate that large optical limiting is possible using thin films of this hybrid material.

Appendix

Personnel supported

Faculty:
M. J. Potasek, PI

Graduate Student:
One

Other:
Ruth Pachter (Research Scientist, Wright Patterson AFB, OH)
S. Kirkpatrick (Research Scientist, Wright Patterson AFB, OH)
D. McLean, Science Applications International, Inc (Dayton, OH)

Publications:

"Effects of Excited State Absorption on Multiphoton Processes", Y. Gao and M. J. Potasek, submitted to Applied Optics.

"High Energy Optical Pulse Beam Width Reduction", Y. Gao and M. J. Potasek, Optical Society of America, Annual conference, accepted.

"Enhancement of Laser Assisted Fabrication of Devices by a Thin Film Two-Photon Absorbing Filter", Y. Gao and M. J. Potasek, Proc. CLEO, Baltimore, MD.

"Enhancement Ablation of Femtosecond Laser Assisted by a Thin Film Two-Photon Absorbing Filter", Y. Gao and M. J. Potasek, submitted to Appl. Phys. Lett.

"Large Nonlinear Optical Properties of Semiconductor Quantum Dot Arrays Embedded in an Organic Medium", Y. Gao, N. Q. Huong, J. Birman and M. J. Potasek, Journal Applied Physics, vol. 96, 4839-4842 (2004).

"Highly effective thin film optical filter constructed of semiconductor quantum dot 3D arrays in an organic host", Y. Gao, N. Q. Huong, J. Birman and M. J. Potasek, Nanofabrication: Technologies, Devices, and Applications, eds. W. Lai, S. Pau. O. Lopez, vol. 5592, 271-281 (2004).

"Equalization of Intensity in a Train of Pulses Using Passive Optical Limiting in a Thin Film", M. Potasek and Y. Gao, Proc. Photonics East, vol 5290, 292-310 (2004).

"Detailed Simulation of Two-Photon Absorption for 3D Micro-Nano Engineering and Patterning", M. Potasek and Y. Gao, Nanofabrication: Technologies, Devices, and Applications, eds. W. Lai, S. Pau. O. Lopez, vol. 5592, 389-399 (2004).

"Numerical Simulations and Modeling for Optical Limiting Materials and Structures with Applications in Laser Protection", M. J. Potasek, Proceedings IEEE Sarnoff Symposium, N.J. March 2003.

"Description and Flowcharts for the User Interface, Computational Methods, and Data Visualization for the Numerical Simulation of 3-D Optical Nonlinear Propagation and Rate Equations Used for Optical Limiters," M. J. Potasek, AFOSR Technical Report, 2003.

"Effects of Multiple Incident Pulses on Optical Limiters Using Excited State Absorbers," M. J. Potasek, AFOSR Technical Report, 2003.

"A Detailed Investigation of Incident Energy on Reverse Saturable Absorbers," M. J. Potasek, AFOSR Technical Report, 2003.

"Description of Numerical Simulations for Optical Limiting Materials and Structures," M. J. Potasek, AFOSR Technical Report, 2003.

"Excited State Absorbers: Materials, Phenomena, Devices, and Numerical Simulations," M. J. Potasek, AFOSR Technical Report, 2003.

"Flowcharts of the Numerical Algorithms for Propagation In Nonlinear Kerr and Reverse Saturable Absorber Materials with Dispersion and Diffraction", S. Kim and M. J. Potasek, AFOSR Technical Report, 2002.

"From Megabits to Terabits: Nonlinear OpticsAt the Frontier of Laser Protection, Information Processing, and Ocular Biomedicine", M. J. Potasek, AFOSR Technical Report, 2001.

"Description of Numerical Simulations for Optical Limiting Materials and Structures", M. J. Potasek, AFOSR Technical Report, 2002.

INTERACTIONS/TRANSITIONS

(a) Participation/presentations at meeting, conferences, etc

- International Symposium on Optical Science and Technology, 49th Annual Meeting, 2-6 August 2004, Denver, Colorado
- Conference on Two Photon Absorbers and Nonlinear Optics, Washington, DC, Jan 20, 2004
- Conference on Lasers and Electrooptics, Baltimore, MD, Oct. 2003
- M. J. Potasek,"From Megabits to Terabits: Nonlinear Optics At the Frontier of Laser Protection, Information Processing,and Ocular Biomedicine", **invited talk**, City College of New York, NY, 2001
- M. J. Potasek, "Numerical Simulations and Modeling for Optical

Limiting Materials and Structure", IEEE Symposium, The College of New Jersey

- Invited presentation on optical limiting at Wright-Patterson AFB, OH, November 22, 2002
- International Conference for Communications, Computing and Controls, Orlando, FL, 31 July-3 Aug. 2003.
- Invited presentation at the IEEE Sarnoff Symposium, N. J., March 2003
- Research, Technologies, and Applications in Biodefense, Wash., D.C. Aug. 27-28, 2003
- ASME 2nd Annual Nano Engineering Conference, New York University, June 20, 2003
- Conference on Lasers and Electrooptics, Baltimore, MD

(b) Consultative and advisory functions

- Consultation and advisory functions to Dr. Ruth Pachter, WPAFB/ML, Dr. Paul Fleitz, WPAFB/ML, Dr. Chris Brewer, WPAFB/ML, Dr. Sean Kirkpatrick, WPAFB/ML.
- Transfer of documentation and results on large optical limiting materials, numerous conference calls and e-mail communications discussing computations on results to researchers at WPAFB, visit to WPAFB for interaction and information on optical limiting, visit to the Major Shared Resource Center –a multimode super computer at WPAFB
- Dr. Sean Kirkpatrick, WPAFB/Materials Lab, calculations on two photon nonlinear absorbers, numerous e-mail communications on the nonlinear behavior of very high two photon absorbers of critical concern to the materials lab at WPAFB

(c) Transitions

- Numerical code and information about material and device design transitioned to AFRL, MLP at Wright-Patterson AFB, OH
- "A Detailed Investigation of Incident Energy on Reverse Saturable Absorbers", M. J. Potasek, AFOSR Technical Report, 2003.
- "Effects of Multiple Incident Pulses on Optical Limiters Using Excited State Absorbers," M. J. Potasek, AFOSR Technical Report, 2003.
- "Description of Numerical Simulations for Optical Limiting Materials and Structures," M. J. Potasek, AFOSR Technical Report, 2003.
- "Description and Flowcharts for the User Interface, Computational Methods, and Data Visualization for the Numerical Simulation of 3-D Optical Nonlinear Propagation and Rate Equations Used for Optical Limiters," M. J. Potasek, AFOSR Technical Report, 2003.

HONORS/AWARDS

- Dr. M. J. Potasek was elected a **SENIOR MEMBER of the IEEE.** She also obtained membership in WOSA (Women in Optics of the Optical Society of America). She is listed in several Who's Who including Who's Who in America, Who's Who in American Women, Who's Who in Science and Technology.
- Invited speaker: IEEE Sarnoff Symposium, N. J., March 2004
- Invited speaker: "Novel Arrays of Nanostructured Semiconductor Organic Materials with Large Third Order Nonlinearity", City College of New York, N.Y., October 2003.
- Best paper award and invited paper/speaker at the International Conference for Communications, Computing and Controls, Orlando, FL, 31 July-3 Aug. 2003.
- Invited speaker: IEEE Sarnoff Symposium, N. J., March 2003